Internal erosion monitored by spatial-temporal pore pressure changes during full-scale field experiments

In review for submission to American Society of Civil Engineers (ASCE) Journal of Geotechnical and Geoenvironmental Engineering

Minal L. Parekh, P.E.[1,3], Wim Kanning, Ph.D.[1], Carolyne Bocovich[1], Michael A. Mooney, P.E., Ph.D.[1], André R. Koelewijn, Ph.D.[2]

[1]Civil and Environmental Engineering, Colorado School of Mines, Golden, Colorado, United States.
[2]Deltares, Delft, Netherlands

Introduction

Earth dams and levees provide flood protection, clean water supply and renewable energy for millions of people around the world. As these structures age, load and demand tend to increase, making continued reliable performance a growing concern. Internal erosion is one of the primary processes threatening the structural health of earthen embankments, yet the mechanisms involved and opportunities to detect the process are not yet well understood (Schmertmann 2000; Foster, Fell, and Spannagle 2000). The objective of this paper is to relate time-lapse dense pore water pressure measurements and geophysical monitoring to the evolution of the piping process in order to enhance monitoring schemes for earthen embankments subject to internal erosion.

The need to understand better the geotechnical behavior and performance of existing earthen dams and levees—in particular related to seepage, internal erosion and subsequent instability—is compelling. Internal erosion results from the transport and migration of soil particles subject to focused seepage or leakage flow and can occur in the embankment, through the foundation and from the embankment into the foundation. This paper focuses on internal erosion in the foundation, also referred to as backward erosion or piping (van Beek et al. 2014) when an internal erosion channel forms from the downstream exit point and progresses backward toward the upstream side, often at the interface between the embankment and the foundation. If the internal erosion channel reaches the upstream side, progressive forward widening of the erosion channel occurs until the embankment breaches (van Beek et al. 2014). Internal erosion initiates when an embankment experiences a critical combination of hydraulic gradient, in-situ stress conditions, soil porosity and permeability. Four stages commonly characterize the internal erosion process (Fell and Fry 2007): 1) Initiation, when particles begin to move with seepage flow; 2) Continuation, when erosion may halt as forces are reduced or conditions impede particles mobility, i.e. as a result of material types, where filter transitions prohibit movement of material; 3) Progression, when a continuous flow channel may form from seepage gradients and open crack or pipe; and 4) Breach/failure, when sudden, rapid, uncontrolled flow is released from the reservoir as the embankment "breaks".

Currently visual observation of seepage or sand boils is often the best indicator of internal erosion; however, whether the observed indicators are precursors to failure, and how much time exists between boil (water or sand) observations and failure, are unclear based solely on observations (van Beek et al.

2010). A review of *dam* incidents and failures shows the first observable signs of internal erosion tend to be at progression, marked by localized concentrated flow transporting soil, and the time to breach may be hours to weeks (or even years) depending on soil characteristics (Fell et al. 2003). For *levees*, sand boils may indicate local heave initiated at much lower head than required for progression, meaning the process self-arrests at the localized boil (van Beek et al. 2014). Understanding observable or measurable indicators in relation to the time development of internal erosion is critical for determining intervention.

The IJkdijk testing program (Koelewijn et al. 2010) is a series of full-scale experiments that offered unique opportunities to collect nearly continuous data using densely spaced geotechnical instrumentation in order to understand the time dependent evolution of internal erosion in earthen structures. Traditional geotechnical instrumentations in the form of piezometers, inclinometers, weirs, etc., are valuable monitoring tools because the measured parameters (pore water pressure, deformation, flow rates) directly relate to performance. For example, laboratory research and modeling studies shows that the internal erosion process is identifiable in local differential pore pressure measurements (Moffat, Fannin, and Garner 2011; Moffat 2002; Fleshman and Rice 2014). In practice, these traditional geotechnical instrumentation methods are limited for identifying incipient failure modes because they are either widely-spaced point measurements (piezometers, inclinometers) or they collect global observations (seepage weirs,) making locating the process difficult.

This paper focuses on relating data from nearly continuously monitored dense geotechnical pore pressure instrumentation and visual observations to the stages of the internal erosion process using results from full-scale IJkdijk embankment tests in October 2009 and September 2012, during which internal erosion initiated and continued. The 2009 test continued to full embankment breach, with noted “local” pressure drops caused by backward erosion (van Beek et al. 2010). In both tests, the initiation of internal erosion and its temporal transitions were apparent in spatially and temporally dense pore pressure measurements, as confirmed by direct observation of sand traces, water boils, and sand boils. Decreases in measured pore water pressure during constant head conditions indicated localized pressure loss as internal erosion initiated at the embankment toe, remotely located from many of the sensors. The rate of pressure loss increased and stabilized in sensors as the erosion process back propagated beyond the sensors and/or stabilized. Evaluation of spatially anomalous pressure change over time and gradient change over time provided further spatio-temporal information about pressure redistribution resulting from internal erosion by highlighting local low-pressure zones.

Continuous geophysical monitoring and remote sensing offered a supplemental approach – spatially and temporally distributed detection and imaging. The challenge for geotechnical engineering is to understand how geophysical monitoring and imaging relate with traditional geotechnical data to characterize earth dam and levee conditions in order to understand performance. The September 2012 IJkdijk testing included embedded fiber optic temperature and strain measurements, passive seismic, acoustic emissions, electrical self-potential (SP) and remote sensing (LiDAR) monitoring. This paper includes comments on geophysical monitoring methods in their ability to identify concentrated seepage and backward erosion in foundation sands during the September 2012 testing.

IJkdijk levee testing program

Between 2007 and 2012 Stichting IJkdijk, an international research cooperative focused on developing and validating new inspection and monitoring technologies for water barriers (http://www.ijkdijk.nl/en/), coordinated studies to understand levee behavior. The IJkdijk is a field facility near the northeast border of The Netherlands where Dutch-led researchers constructed and loaded levee embankments to study a variety of failure mechanisms and to enable testing of sensor technologies for monitoring levee response (Koelewijn et al. 2010; Zwanenburg et al. 2012). Referenced as T2009 and T2012 in this paper, IJkdijk experiments in 2009 and 2012 addressed the internal erosion failure mode, specifically backward erosion in sandy foundation materials beneath a clay embankment, the focus of this paper. While both tests included densely spaced sensors to study pore water pressure distribution, T2009 (the second of four tests performed in 2009) focused on investigating the failure process to validate the Sellmeijer erosion model to identify the critical head for piping (H. Sellmeijer et al. 2011). T2009 progressed to full embankment breach (Koelewijn et al. 2010; van Beek et al. 2010). T2012 included a vertical geotextile installed on the downstream side of the embankment at the interface between clay embankment and sand foundation materials and extending into the foundation as a potential backward erosion mitigation measure. T2012 did not progress to full embankment breach but included higher reservoir heads than T2009.

For both T2009 and T2012, the test embankments comprised moisture-conditioned and compacted clay (CH, per Unified Soil Classification System (USCS)), with plasticity index (PI) ranging from 50 to 60 and liquid limit (LL) ranging from 80 to 90. Test embankment height in T2009 was 3.5 m and in T2012 was 4 m. The embankment rested on a poorly graded sand (SP, per USCS) foundation for both T2009 and T2012. The foundation sand in T2009 had mean grain size (d_{50}) of 0.21 mm, uniformity coefficient (c_u) of 1.8, and relative density after placement (D_r) of approximately 92 percent (van Beek, de Bruijn, and Knoeff 2009). In T2012, the upper 0.5 m foundation sand had d_{50} of 0.18 mm, c_u of 1.7, and D_r of approximately 92 percent and the lower 2.5 m had d_{50} of 0.18 mm, c_u of 1.8, and D_r of approximately 50 to 60 percent (van der Kolk 2013). In both tests, a geomembrane isolated the constructed embankment and foundation from the influence of outside soil and groundwater. The facility included a membrane-lined upstream reservoir to provide hydraulic loading on the embankment, and a membrane-lined constant-head downstream reservoir, equipped with an outflow gaging station. The foundation sands were saturated prior to the start of any hydraulic loading (van Beek, de Bruijn, and Knoeff 2009). Pumps transferred water from a nearby source (a ditch on the west edge of the site) to the upstream reservoir to achieve the intended stepwise hydraulic load. During time periods between reservoir level increases, pumps were off, resulting in slight head decreases during holding periods.

For T2009, 120 pore water pressure sensors arranged in eight rows of 15 (Figure 1) recorded pore water pressures just below the interface between the clay and the sand. A data logger recorded the pressures at approximately 5-sec intervals for the duration of the testing (approximately 151 hrs.) Analyses exclude several of the sensors that did not collect reliable data, as reflected in Figure 1.

For T2009, Figure 2 shows the increases in water level and the visual observations. The downstream water level was generally constant, set at zero datum, so that the head difference was equal to the upstream water level. Sand traces (isolated cloudy streams measuring on the order of mm to cm in the

downstream toe with little observable change in local flow or particle movement) occurred at upstream head from 0.4 to 1.5 m. Water boils (localized features of concentrated outflow measuring on the order of cm in the downstream toe where upward seepage lifted sand particles but did not transport or deposit particles in a crater) occurred at an upstream head of 1.5 m (25 hrs elapsed) and sand boils occurred at head of 1.6 m (28 hrs elapsed), as shown in Figure 2. The upstream water level was held relatively constant at 1.6 m until the sand boils stabilized (from 28 to 48 hrs elapsed). The level increased by 0.1 m, with each increase held for 10 hrs to 1.9 m (66 hrs elapsed.) The upstream level remained at 1.9 m from 66 to 126 hrs. Forward progressive erosion, the widening of the initial erosion channel once it reaches the upstream (van Beek et al. 2014), began at 95 hrs elapsed time, and the embankment started cracking at 116 hrs elapsed. Full breach occurred near the east abutment at upstream head of 2.1 m (137 hrs elapsed.)

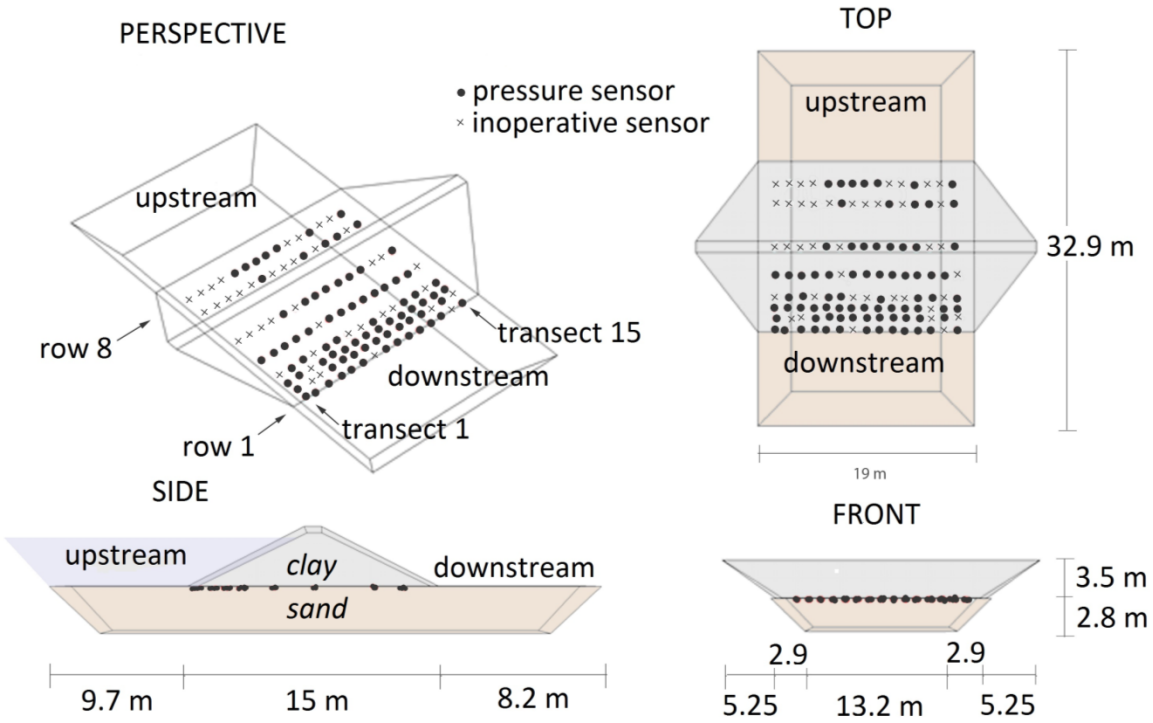

Figure 1 T2009 embankment configuration and pore water pressure sensor locations.

While the embankment configuration was similar for T2009 and T2012, the primary difference was that T2012 included installation of a vertically oriented geotextile strip near the downstream toe of the embankment as a potential internal erosion mitigation method, shown in Figure 3. For T2012, 35 pore water pressure sensors arranged in four rows recorded pore water pressures just below the interface between the clay and the sand. Ten sensors measured pressures at the bottom of the geotextile (approximately 0.5 m below the clay-sand interface) on both sides of the geotextile. Analyses exclude three of the top sensors which did not collect reliable data, as reflected in Figure 3.

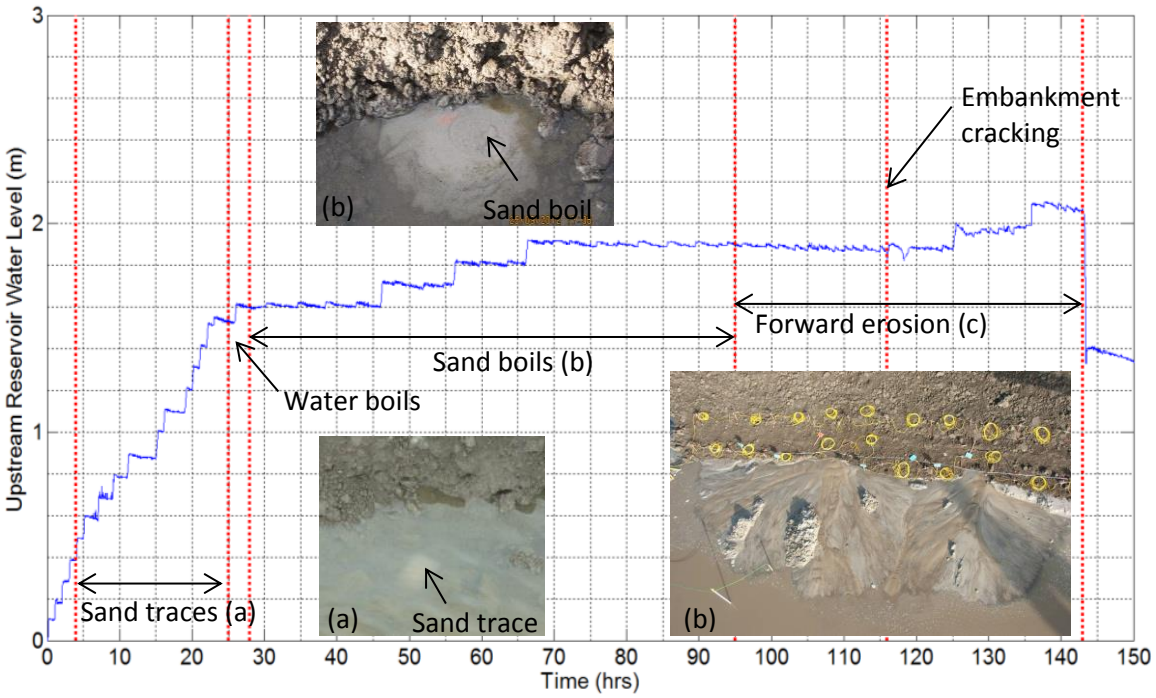

Figure 2 T2009 loading schedule annotated with visual observations. Example photos of (a) sand traces, (b) sand boil, and (c) forward erosion. The downstream water level is set as the zero datum.

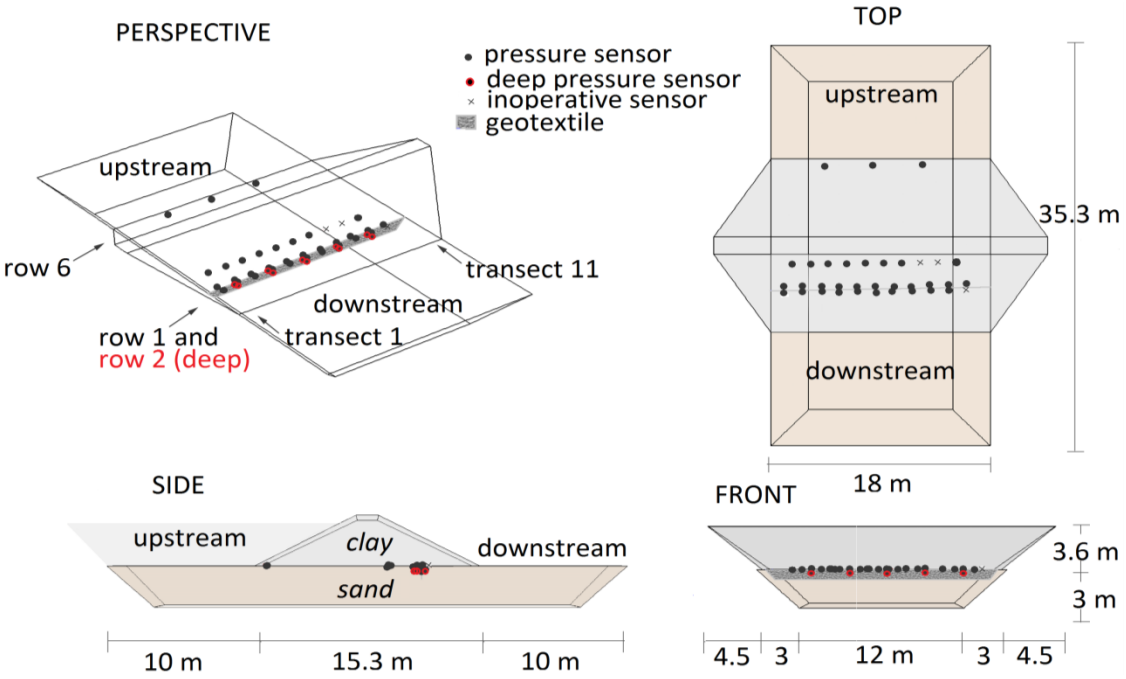

Figure 3 T2012 embankment and geotextile configuration and pressure sensor locations.

The loading schedule changed for T2012, designed to exceed the critical head as determined in the T2009 failure in order to test the geotextile as an internal erosion mitigation method (Forster 2013). For T2012, the water level upstream of the embankment increased to 0.5 m and remained at that level for approximately 8 hrs until outflow rate steadied. Water level then increased to 1 m until outflow steadied (approximately 5 hrs,) then to 2 m. Water and sand boils occurred during the increase at head of 1.6 m (18 hrs elapsed), as shown in Figure 4. The upstream water level was held relatively constant at 2 m until the sand boils appeared to stabilize (22 to 30 hrs elapsed.) From there, the upstream reservoir level rose to approximately 3.25 m (38 hrs elapsed), and eventually to 3.6 m (90 hrs elapsed.)

As noted in Figure 4, the T2012 embankment exhibited: observable cracking at 20 hrs elapsed with cracks stabilizing at 64 hrs; seepage along the abutments at 40 hrs; and through-seepage (likely through clay clods and at boundaries between construction lifts) and softening of foundation materials (measuring on the order of meters) at the embankment toe at 90 hrs. Full breach did not occur in this test, with a maximum upstream head of 3.6 m as limited by the banks of the upstream reservoir (total test time 142 hrs.)

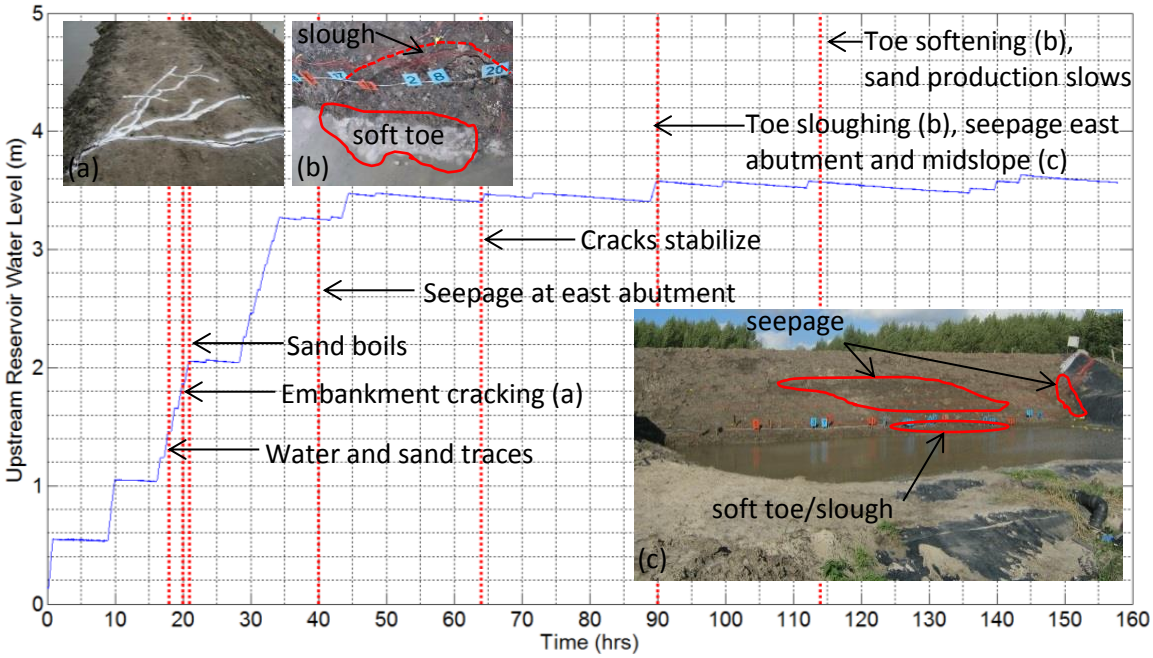

Figure 4 T2012 loading schedule annotated with visual observations.

The visual observations of sand boils serve as ground truth to the indicators of internal erosion given by measurements from the pore pressure sensors. Figure 5 represents the approximate locations of sand boils in plan view and representations of sand boil activity for both T2009 and T2012. For T2009, the plot visually presents two stages of sand boil activity qualitatively: the first appearance of sand traces or localized preferential flow, and growing sand boils depositing sand material in a crater around a hole. Sand production was greatest on the east side of the embankment, which coincides with the embankment breach. For T2012, the plot provides a quantitative cumulative summary, with line thickness varying with relative cumulative mass removed based on field measurements. Water and

sand boils appeared at approximately 18 hrs, with the amount of sand removal concentrated near the center of the embankment. Sand boil production was greatest near the center of the T2012 embankment (approximately 5 to 11 m from the southwest toe of the embankment.)

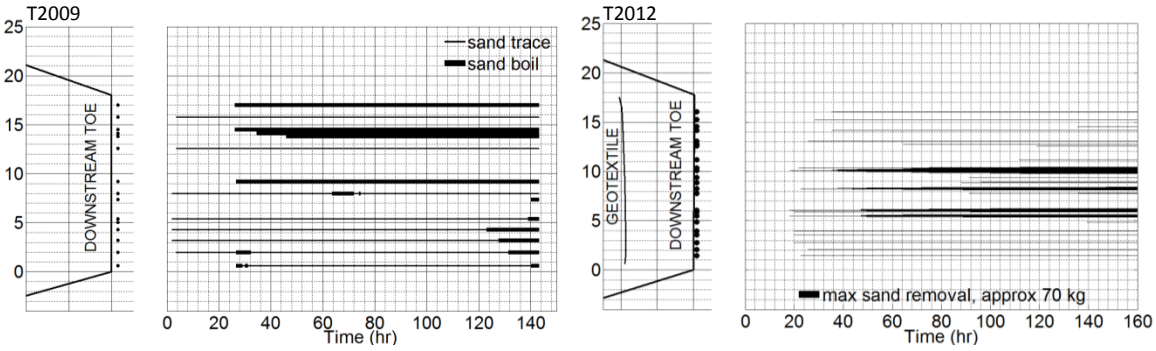

Figure 5 Sand boil approximate locations, sand production for T2009 (left), and T2012 (right). For T2009, sand boil production is represented in 2 stages: sand trace or water boil with little to no sand particle migration, and full sand boils depositing material in a growing "crater." For T2012, sand boil production is represented with varying line thickness as relative cumulative mass removed, based on quantitative field measurements.

Geophysical Observations (T2012)

T2012 included deployment of a nearly continuous monitoring system involving passive electric (SP), passive seismic and acoustic emissions, and terrestrial remote sensing sensors for light detection and ranging (LiDAR.) Each of these methods identified possible concentrated seepage and internal erosion at various times during the experiment.

Acoustic emissions analysis of vibrations measured on the surface of the downstream embankment slope indicated increased emissions activity near the center of the embankment toe apparent around 55 hrs (Mooney et al. 2014). A separate acoustic emission analysis to localize sources showed coherent sources originating from within a search grid at the interface between the sand and clay starting near 50 hrs (Rittgers et al. 2014), corresponding spatially and temporally with increased sand boil activity. Acoustic source localizations became more coherent and consistent near the center of the downstream embankment toe and grew progressively more coherent and consistent in time. SP analysis of changes in the passive electrical fields caused by water through the porous soil material indicated concentrated seepage flow through the embankment at 99.6 hrs near the center of the downstream toe (Rittgers et al. 2014; Mooney et al. 2014; Rittgers 2013). Passive seismic analysis using ambient noise (seismic interferometry) to interrogate the embankment for structural changes indicated a compressive wave velocity drop associated with the increase in upstream water level (and decrease in effective stress) at 45 to 50 hours (Planes et al. 2015). Additional velocity reductions were apparent at 64 hr and 72 hr, concurrent with additional upstream water level increases. The LiDar analysis identified settlement at the embankment flanks starting at 25 hrs and sloughing because of instability at the embankment toe at 108 hrs (Mooney et al. 2014). Fiber optic cables mounted to geotextiles installed horizontally at the clay-sand interface (Artieres and Dortland 2013) measured temperature and strain at four alignments parallel to the dam crest. Fiber optics installed on the vertical geotextile used as internal erosion mitigation near the downstream toe of the embankment measured temperature and strain

perpendicular to seepage flow from 0.5 m above to 0.25 m below the clay-sand interface. The processed temperature data indicated seepage from onset of the increase in upstream reservoir level. At nearly 48 hrs, temperature data showed seepage increasing on the west side of the embankment, but by the next day, the temperatures were uniform, indicating more uniform flow through the foundation. Strain measurements indicated movement at the clay-sand interface near the east abutment (a zone approximate 16 m from the west end of the downstream toe) 48 hours into testing, corresponding temporally with increase in sand boil activity. Strain increased slightly at the clay-sand interface over the next 3 days, and strain measured on the vertically installed cables indicated movement in the clay approximately 0.3 m above the clay-sand interface, and in the sand to a depth of 0.25 m concentrated near the east abutment (a zone approximately 14 m from the west downstream toe.) (Artieres and Dortland 2013)

Analysis of groundwater contours

Continuous pore pressure measurements from a dense array of piezometers allow a detailed spatial analysis of seepage and internal erosion. Figure 6 presents time-lapse images of both T2009 and T2012 groundwater pressure contours. The plots extrapolate pressures to cover the whole levee. The T2009 contours indicate a low-pressure zone near the center region of the embankment downstream toe (77 hrs), possibly indicating initiation of internal erosion. The low-pressure zone propagates backward from downstream to upstream (95 hrs), possibly indicating continuation of internal erosion. Near the end of T2009, a zone of increased pressure concentrates near the center region of the upstream embankment (126 hrs) possibly indicating further continuation of internal erosion and leading to embankment breach.

The T2012 contours indicate low pressure back propagating in isolated “fingers” in the downstream toe. However, in contrast to the T2009 groundwater contours, the T2012 contours change little between 52 to 137 hrs. These measurements reflect that the back propagation of low pressures and internal erosion was limited and did not result in breach, possibly because the geotextile served to mitigate the internal erosion process.

Normalized pressure trends: temporal response

A significant finding in both T2009 and T2012 data is that pore water pressure measurements in the sand layer upstream of the downstream toe decreased as internal erosion initiated at the downstream toe. The pore water pressure measurements, and in some cases the rate of pressure decrease, changed with time as downstream internal erosion propagated backward, even in sensors located far from erosion activity.

Figure 7 illustrates this behavior by presenting time-lapse pore water pressure measurements from one transect of piezometers in T2009 and T2012. Pore water pressure values are shown normalized by the upstream reservoir head. In T2009 during rapid initial loading (t = 0 to10 hrs), the pore water pressures increase with the upstream reservoir head. The normalized pressures closest to the upstream reservoir increase proportionally (resulting in a relatively flat line, $dP/dt = 0$) while the downstream

pressure sensors measure a slight positive trend. The response of the normalized readings in this early time range is noisy because of the rapid change in upstream reservoir head and the lag time to sensor response. In T2012 during initial loading, the normalized pore water pressure response is proportional to the upstream reservoir head.

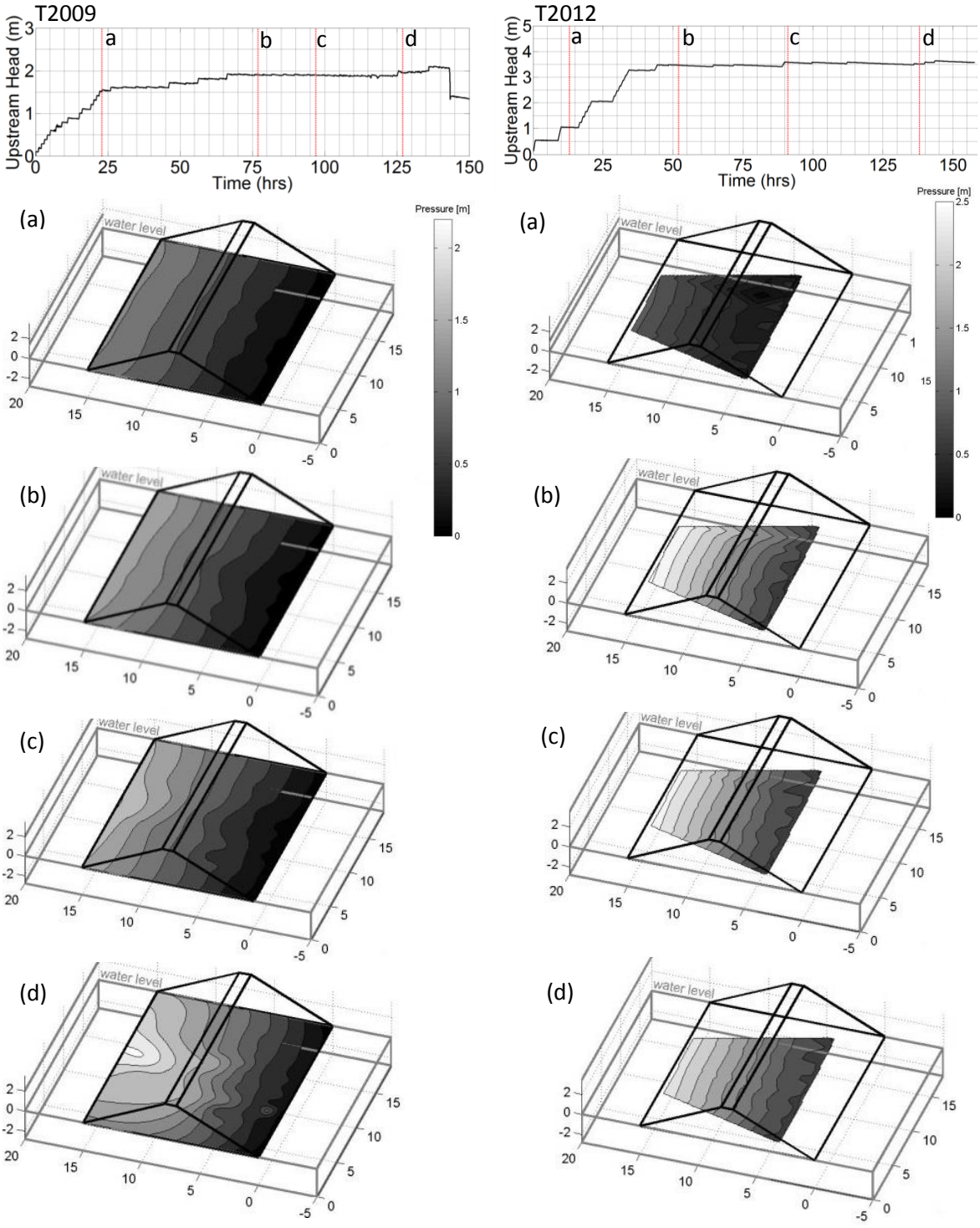

Figure 6 Pore pressure distribution at various upstream reservoir levels, T2009 (left) and T2012 (right).

Each T2009 and T2012 pore water sensor showed a decrease in normalized pore water pressure. This behavior is anomalous because in theory, normalized pore water pressure remains constant during steady state seepage. The initiation of the pore water pressure decrease, marked as ***f*** for each sensor in Figure 7, followed the visual observation of sand traces (t=5 hrs) in T2009 and sand boils (t=18 hrs) in T2012. Sand traces represent localized particle movement with limited pressure influence, initiating the formation of a pipe and anomalous pore pressure changes. In T2009, the noisy normalized pore water pressures measured closest to the upstream reservoir make identifying this initiation point challenging; the transition ***f*** may be occurring earlier in the signal, but the analyses include the first identifiable transition to a decreasing pressure trend.

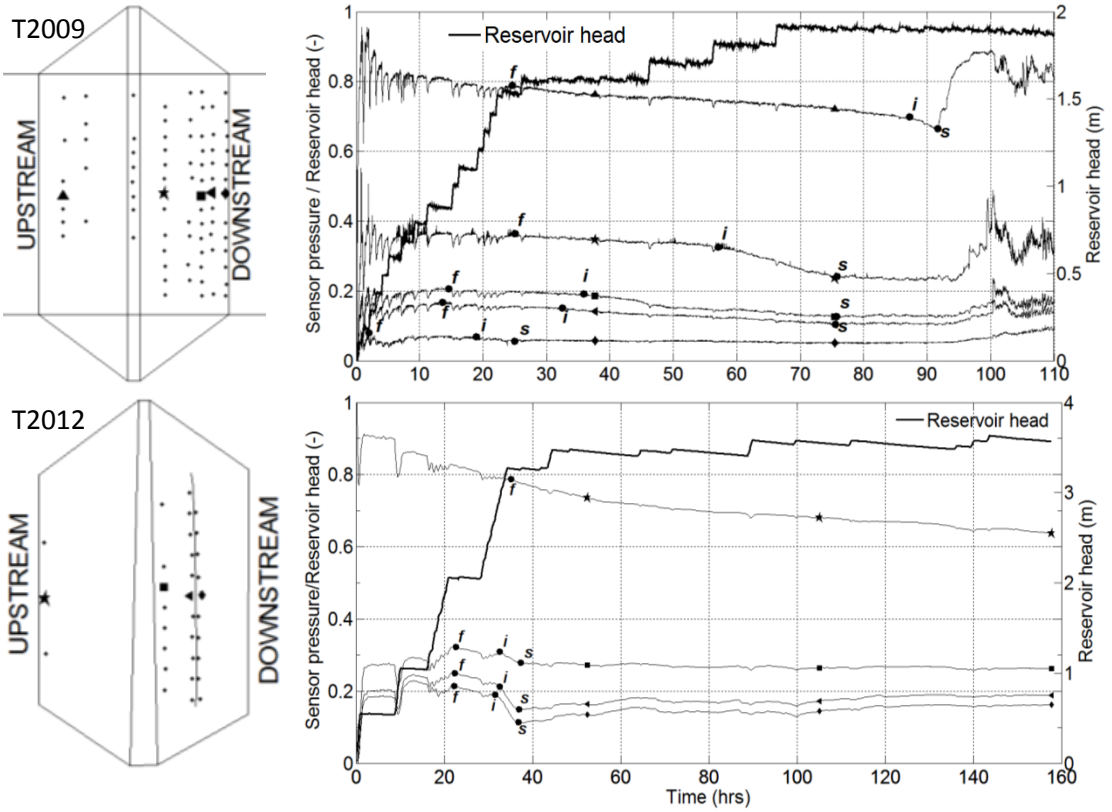

Figure 7 Pressure measurements normalized to upstream head T2009 (top) and T2012 (bottom) for transect near embankment center.

In many of the sensors, the anomalous pore water pressure decreases were followed by a marked— more rapid— increase in pressure loss with time (-dP/dt). This change is marked as ***i*** in Figure 7 for the sensors demonstrating this behavior. The marked increase in pressure loss corresponds with the visual observation of increased sand production from sand boils (t=20 to 60 hrs) in T2009 and (t≈35 hrs) in T2012. The increase in pressure loss and the increase in sand boil activity indicate that resistance to flow is decreasing because of the erosion of sand and deposition at the toe.

In some sensors in both T2009 and T2012, the pore water pressure stabilized, denoted as ***s*** in Figure 7 for the sensors demonstrating this behavior. In T2009, the stabilization was not apparent in the

upstream-most sensors between the marked increase in pressure loss and forward erosion and breach, perhaps because of the short time period. In T2012, the upstream water level increased quicker and to a higher ultimate level (by 1.5 m) than in T2009 but the embankment did not breach. The faster loading resulted in faster normalized pressure response with little time lag between the ***f***, ***i*,** and ***s*** transitions. In T2012, the pore pressure sensors furthest upstream did not exhibit the marked increase in pressure loss or stabilization, but instead pressures continued to drop steadily for the duration of the experiment. In T2012, the stabilization was followed by slight pressure increases in many of the downstream sensors. As shown in Figure 5, new sand boils appeared later in the test (t=90 to t=140). These combined behaviors indicate that within the interval of the T2012 test, the conditions did not reach equilibrium.

The transitions in the temporal pressure trends can relate the pressure measurements to the stages of internal erosion. The transition to steady pressure drop (***f***) could indicate the *initiation of internal erosion* at location(s) downstream of the sensor if the sensor is within a zone of influence of the erosion feature. The increase in pressure drop (***i***) could indicate *the continuation of internal erosion*, with erosion features downstream of the sensor changing such that resistance to flow is decreasing more quickly (i.e. erosion features backward propagating closer to a sensor, but not necessarily at the location of the sensor.) Pressure stabilization (***s***) occurs when conditions downstream of the sensor no longer influence pressure changes, perhaps because internal erosion channel(s) have reached the sensor such that the sensor is connected hydraulically to the downstream reservoir and no further pressure drop can occur. The stabilized pressure at a sensor may not be equal to the downstream reservoir head because of flow resistance within the erosion channels, as reflected in studies modelling the process (J. B. Sellmeijer 1988). In this case, stabilization occurs as the internal erosion continues further upstream from the sensor. Alternatively, stabilization could indicate that conditions downstream of the sensor have steadied for other reasons, such as the cessation of internal erosion because of mitigating factors (geotextile, in the case of T2012.) Lack of stabilization indicates that sensors are influenced still by pressure changes occurring downstream, meaning downstream pressure redistribution, and therefore, internal erosion, may be ongoing.

Phases of Detection in Time and Space

Mapping the pressure transitions identified in all sensors provides insight into the spatio-temporal evolution of internal erosion channels. Figure 8(a) spatially represents the time at which the marked increased pressure loss (***i***) began in each of the T2009 sensors, and Figure 8(b) spatially represents the start of stabilization (***s***) time in each of the T2009 sensors. The initial pressure loss (***f***) is not represented, as this point was not discernable for some of the sensors because of the signal noise. In Figure 8(a), marked pressure loss began earlier in two zones (circled) than in the rest of the embankment and stabilization began earlier in the center zone (circled) as well. These two representations provide a spatial sense of the zone of influence of pressure changes caused by the initiation of internal erosion in T2009. Mapping the times of stabilization in T2009 indicates the approximate length of the erosion channel(s). Evaluating the time lag (Figure 8(c) and (f)) between the two phases provides some indication of the look-ahead time between recognizable downstream pressure drop (caused by internal erosion initiation) and stabilization. These visualizations also demonstrate a wide zone of pressure

influence for the internal erosion in T2009. Note the plots use extrapolated data in the absence of measured data (upstream edges.) Where the data did not exhibit a clear transition between pressure response behaviors, a transition time was not included in the analysis, resulting in gaps in the T2012 plots Figure 8 (d) and (e), which represent the time of the start of increased pressure loss (***i***) and the time of stabilization (***s***,) respectively. The T2012 contour plots indicate that pore water pressure stabilization occurred beneath only a portion of the structure. T2012 did not progress to full breach, perhaps because the presence of the geotextile served to mitigate the internal erosion process by limiting particle mobility. The geotextile likewise may have influenced the pressure distribution by causing complex (three-dimensional) flow, local or widespread pressure build up and/or pressure relief, behavior that did not equilibrate in the interval of the experiment.

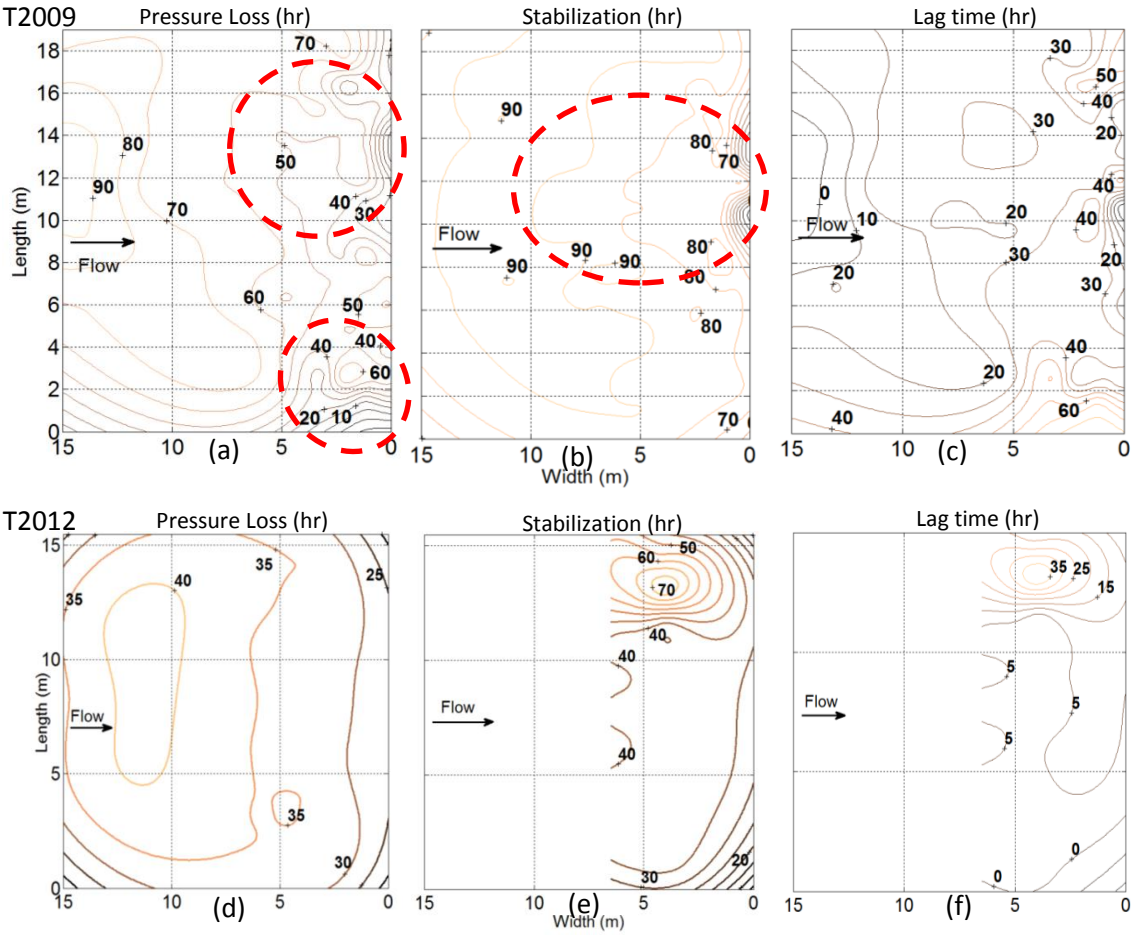

Figure 8 Spatial representation of T2009 (top) and T2012 (bottom) of time to reach pressure loss and time to stabilize. The difference between (a) and (b) is shown in (c) and the difference between (d) and (e) is shown in (f), the lag time between pressure loss and stabilization.

Pressure trends within longitudinal rows

Another finding in both T2009 and T2012 data is in variability in the pressure response with time (dP/dt) along longitudinal sections (i.e. within sensor rows,) as shown in Figure 9. In an idealized

homogenous earthen structure under steady state seepage, water flow would be uniform, so pressures measured along the same longitudinal alignment would also be the same. The variations in the pore water pressure response indicate spatial variability in the flow conditions. The times when sensors start responding differently from each other within a row indicate the times at which local pressures were decreasing or increasing. Pressure decreases occurred because of increased hydraulic conductivity (i.e. internal erosion channels); pressure increases could have occurred as a result increase resistance to flow (i.e. self-healing or downstream clogging.)

Figure 9 presents the pressure response from sensors in the row nearest to the downstream toe for both tests. In the downstream row in both T2009 and T2012, pressure response began to spread at about 20 hrs and 30 hrs respectively, indicating spatial variability in flow. To examine pressure response (dP/dt) for T2009, the response was calculated as the deviation from the average response for all sensors in the row in 1-hr sliding windows. Figure 10 shows T2009 sensors in row 1 at the center of the embankment responded slower (lower dP/dt than average response in the row) to pressure increase from 20 to 30 hrs, reflecting the lower pressures near the center of the embankment downstream toe. The time and location were coincident with the start of sand boil production (Figure 5.) In row 3, sensors 8 and 9 responded slower to pressure increase from 40 to 70 hrs, reflecting the lower pressures near the center of the embankment downstream toe as internal erosion worked to equilibrate pressures to the downstream reservoir level.

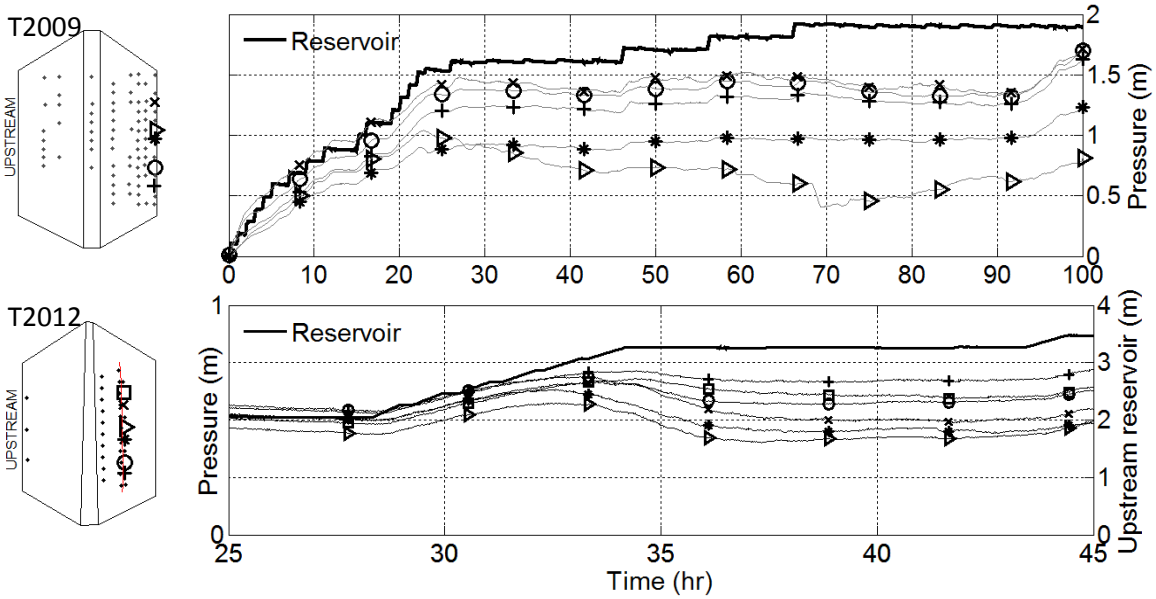

Figure 9 Pressure plotted for T2009 (top), truncated at 100 hr. Pressures plotted for 2012 (bottom), truncated from 25 to 45 hr.

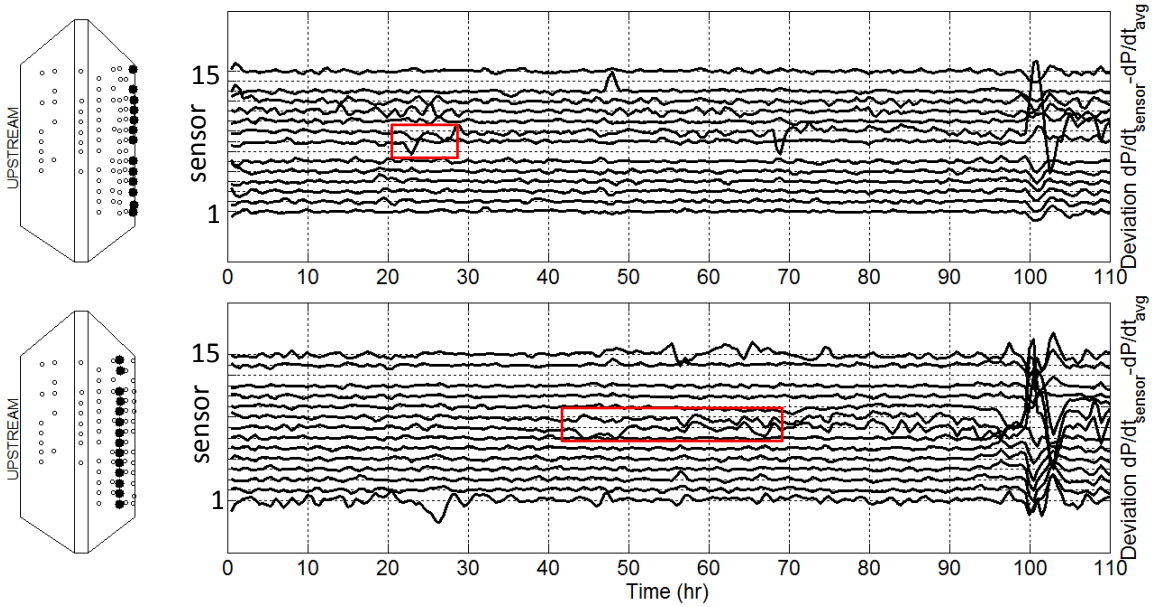

Figure 10 Sensors in T2009 test row 1 (top) and row 3 (bottom) with pressure response depicted as deviation from average row response. Pressure response (dP/dt) calculated in 1 hr sliding windows.

In T2012, sensors at the embankment center responded slower to pressure increases between 30 to 40 hrs, as shown in Figure 11. Variation in response within the row of piezometers started near the center with lower pressures in these middle sensors and higher pressures toward boundaries, reflecting the lower pressures near the center of the embankment downstream toe. The lower pressures were coincident in time and location with the start of sand boil production (Figure 5).

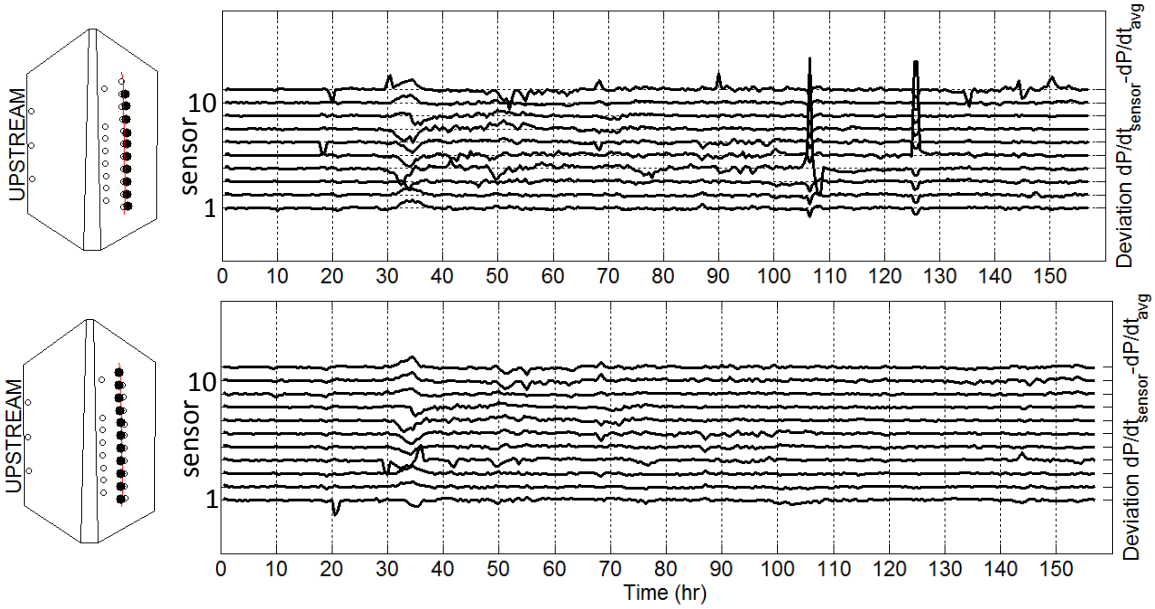

Figure 11 Sensors in T2012 test row 1 (top) and row 3 (bottom with pressure response depicted as deviation from average row response. Pressure response (dP/dt) calculated in1 hr sliding windows.

Gradient trends

Gradient (dH/L, with L the distance between rows) analysis reveals spatial variation and trends in local gradient. Figure 12 presents T2012 gradients between sensor pairs in downstream adjacent rows. Evaluating the gradient along the embankment alignment at various locations under the embankment showed steeper gradient near the center of the embankment downstream. The increased gradient resulted from the downstream pressure drop caused by internal erosion features. In T2012, gradients at transect 6 increased more than the others at approximately 18 hours, and gradients at transects 3 and 4 were higher than the others at approximately 35 hrs.

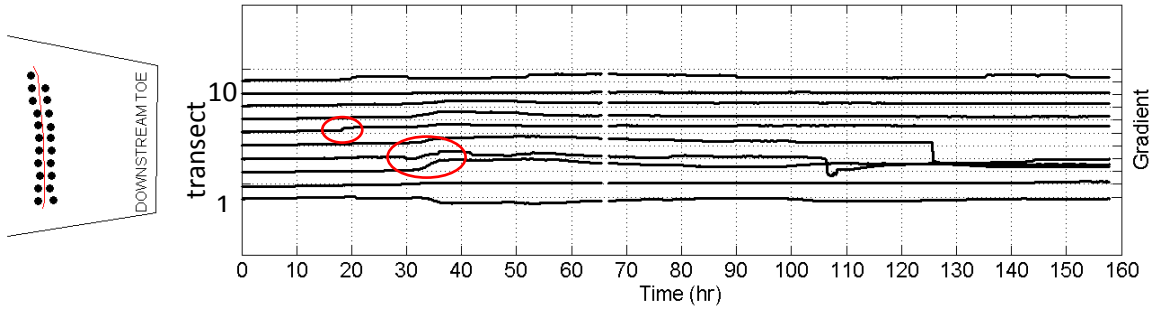

Figure 12 T2012 time variant gradient between two rows of sensors plotted for transects along the embankment length

Evaluating gradients along transects of the T2009 embankment showed the gradient peaked at the downstream toe at about the same time as boils appear, as shown in Figure 13. The gradient peak back propagated through the sensor transect, providing an indication of rate of movement of channels in cross section, as noted in previous analyses. (van Beek, de Bruijn, and Knoeff 2009) In T2012, however, the gradient peaks occurred at nearly the same time, as shown in Figure 13.

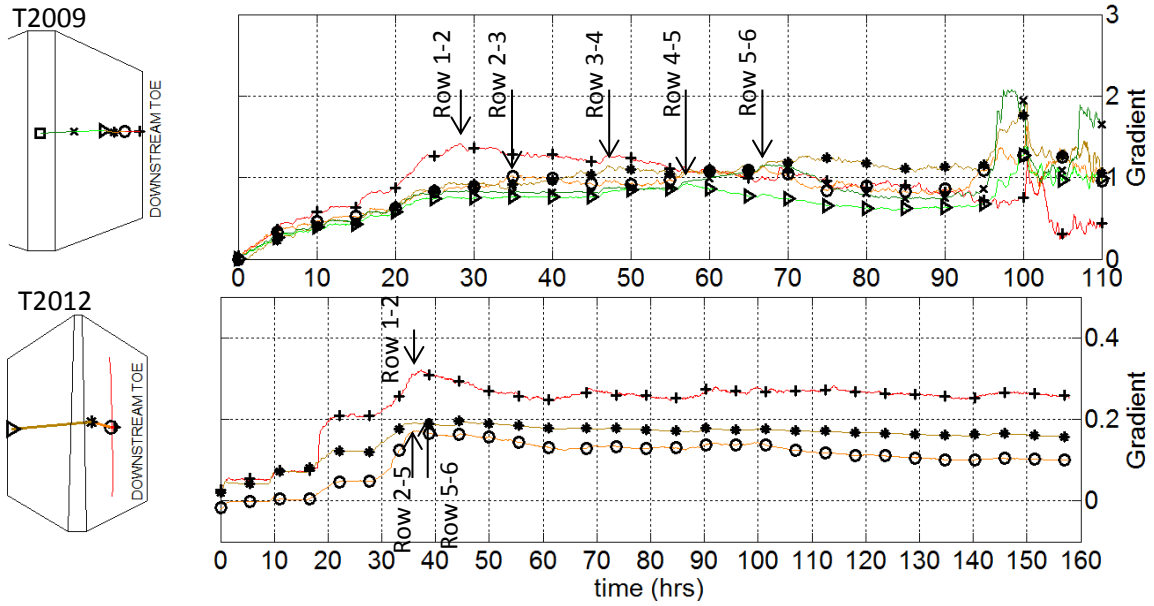

Figure 13 T2009 time variant gradient in cross section, truncated at 110 hrs (top). T2012 time variant gradient in cross section (bottom.)

Effect of the geotextile: T2009 to T2012

The differences between T2009 results and T2012 results are affected largely by the presence of the geotextile and its effect on flow and pore water pressure distribution. The effect of piping zones that arrest at the geotextile on the flow characteristics are not yet fully understood, but the pressure distribution patterns observed in T2009 were truncated in T2012, and breach did not occur despite a significantly higher upstream reservoir head.

In both T2009 and T2012, pore water pressure dropped in some sensors at times corresponding approximately with the first observed water boils. However, in T2012, the pressures downstream of the crest decreased and stabilized more quickly than in T2009. In T2009 pore pressures started decreasing at the downstream toe and the pressure drops propagated back toward the upstream reservoir, followed by a rapid forward-propagating increase in pore water pressure from the upstream reservoir to the downstream reservoir. The forward pressure propagation marked forward erosion, followed by full embankment breach. In T2012, downstream pressures did drop, but backpropagation was limited and forward pressure propagation from the upstream reservoir did not occur, confirming that forward erosion did not occur. The geotextile likely influenced the limited movement of particles, and therefore limited the backward extent of pressure drop, and the backward propagation of internal erosion. Increases in pore pressure (apparent both downstream and upstream of the geotextile) in T2012 could have been the result of geotextile clogging or other complex three dimensional flow effects caused by the geotextile.

Conclusions

This study evaluated two sets of pore pressure data from full-scale IJkdijk experiments to study internal erosion in earthen embankments. T2009 tested the embankment to failure, while T2012 included a geotextile to mitigate internal erosion and the embankment did not breach. The pore pressures were studied extensively to gain better knowledge about internal erosion and indicators of internal erosion progression in pore water pressure data. Temporally and spatially dense pore pressure measurements detect the initiation and continuation of internal erosion, even in sensors remotely located from the internal erosion event(s.) Spatial and temporal changes in pore water pressure correlate with visual observations.

Pore pressure contour plots for T2009 show back propagation of decreasing pore pressure followed by forward propagation of pore pressure measurements, coincident with the observed breach and failure times. Pore pressure contour plots for T2012 show decreasing pore water pressure up to a spatial and temporal barrier, possibly due to the geotextile preventing migration of sands and propagation of internal erosion. The pore pressure analyses show three transitions in measured pressures at a given sensor:

1. Initial decrease in pressures measured by sensors upstream of internal erosion;
2. Marked increase in pressure loss as erosion channel approaches sensor location;
3. Stabilization of pressure as the erosion channel stabilizes.

Further analysis includes studying pressure trends, anomalous pore pressure behavior along the length of the levee, and gradient trends across the levee. The anomalous pore pressure behavior, both at the toe and upstream of the toe, correlate with the sand boil progression. As sand traces, water boils, and sand boils appear, pore water pressures start to decrease at the downstream toe. As sand production increases, the pressure decrease propagates toward the upstream reservoir. The initial pressure drop occurs coincident with the first sign of sand traces, the first sign of the initiation of internal erosion. Marked increase in pressure loss over time occurs coincident with sand boil production increases. In T2009 local pore pressure stabilization indicates continuation of erosion beyond stabilized sensors. In T2012, the absence of stabilization indicates that the pressures do not come to equilibrium during the testing interval. Areas with the highest pore water pressure drop (or higher gradients) are near the sand boils producing the most sand. Pressure changes over time within sensor rows reveal windows in time and locations where pressure response is slow, coincident with areas of low pressure and sand boil production.

Recommendations for further research include determining the applicability for pore water pressure and geophysical methods for early detection of internal erosion for feasible field (sparser instrumentation) monitoring; evaluating the magnitude and spatio-temporal change in hydraulic conductivity in the foundation caused by internal erosion; and, relating the measurements to internal erosion models.

Acknowledgements

The researchers gratefully acknowledge Deltares and Stichting FloodControl IJkdijk in the Netherlands for providing access to the IJkdijk site and for sharing the data from 2009 and 2012 experiments.

Funding for this study was provided in part by the National Science Foundation under the SmartGeo Program (Project IGERT: Intelligent Geosystems; DGE-0801692), the Partnerships for International Research and Education (PIRE) Program (PIRE: Advancing Earth Dam and Levee Sustainability through Monitoring Science and Condition Assessment; OISE-1243539), the Office of Energy Efficiency and Renewable Energy (EERE), U.S. Department of Energy, (Award Number DE-EE0002668), and the Hydro Research Foundation.

The information, data or work presented herein was funded in part by an agency of the United States Government. Neither the United States Government nor any agency thereof, nor any of their employees, makes and warranty, express or implied, or assumes and legal liability or responsibility for the accuracy, completeness, or usefulness of any information, apparatus, product, or process disclosed, or represents that its use would not infringe privately owned rights. Reference herein to any specific commercial product, process, or service by trade name, trademark, manufacturer, or otherwise does not necessarily constitute or imply its endorsement, recommendation or favoring by the United States Government or any agency thereof. The views and opinions of authors expressed herein do not necessarily state or reflect those of the United States Government or any agency thereof.

References

Artieres, O., and G. Dortland. 2013. Survey towards the Functionality of Geotextiles as Piping Prevention Measure, Monitoring Piping Prevention with the TenCate GeoDetect Smart Filter. TenCate, Inventec B.V.

Fell, R., and J. J. Fry, eds. 2007. Internal Erosion of Dams and Their Foundations. London UK: Taylor & Francis.

Fell, R., C. F. Wan, J. Cyganiewicz, and M. Foster. 2003. "Time for Development of Internal Erosion and Piping in Embankment Dams." Journal of Geotechnical and Geoenvironmental Engineering ASCE 129 (4): 307–14.

Fleshman, M., and J. Rice. 2014. "Laboratory Modeling of the Mechanisms of Piping Erosion Initiation." Journal of Geotechnical Engineering, ASCE 140 (6).

Forster, U. 2013. Research into the action of geotextiles as piping inhibitory action (Main Report) (Onderzoek naar de werking van geotextielen als pipingremmende maatregel (Hoofdrapport)). 1206806-000-GEO-0014. Deltares.

Foster, M., R. Fell, and M. Spannagle. 2000. "The Statistics of Embankment Dam Failures and Accidents." Canadian Geotechnical Journal 37 (5): 1000–1024.

Koelewijn, A., G. de Vries, H. van Lottum, U. Forster, V. van Beek, and A. Bezuijen. 2010. "Full-Scale Testing of Piping Prevention Measures: Three Tests at the IJkdijk." In Physical Modelling in Geotechnics. Zurich, Switzerland: Taylor & Francis.

Moffat, R. 2002. "A Laboratory Study of Particle Migration in Cohesionless Soils." Dissertation, Vancouver, B.C., Canada: University of British Columbia.

Moffat, R., R.J Fannin, and S. Garner. 2011. "Spatial and Temporal Progression of Internal Erosion in Cohesionless Soil." Canadian Geotechnical Journal 48 (3): 399–412.

Mooney, M. A., M. L. Parekh, B. Lowry, J. Rittgers, A. R. Koelewijn, A. Revil, and W. Zhou. 2014. "Design and Implementation of Geophysical Monitoring and Remote Sensing during a Full Scale Embankment Internal Erosion Test." In Geo-Characterization and Modeling for Sustainability, Geo-Congress 2014. Atlanta, GA: ASCE.

Planes, T., M. A. Mooney, J. B. Rittgers, M. L. Parekh, M. Behm, and R. Snieder. 2015. "Time-Lapse Monitoring of Internal Erosion in Earthen Dams and Levees Using Ambient Seismic Noise." Geotechnique (in Review).

Rittgers, J. B. 2013. "Geophysical Trends Apparent During Cracking, Erosion, and Self-Healing of Soils during Lab-Scale and Full-Scale Tests." presented at the SAGEEP Conference, Denver, Colorado, March.

Rittgers, J. B., A. Revil, T. Planes, M. Mooney, and A. Koelewijn. 2014. "4-D Imaging of Seepage in Earthen Embankments with Time-Lapse Inversion of Self-Potential Data Constrained by Acoustic Emissions Localization." Geophysical Journal International 200 (2): 758–72. doi:10.1093/gji/ggu432.

Schmertmann, J. 2000. "The No-Filter Factor of Safety Against Piping Through Sands." Geotechnical Special Publication No. 11 Judgement and Innovation, The Heritage and Future of the Geotechnical Engineering Profession, 65–132.

Sellmeijer, H., J. L. de la Cruz, V.M. van Beek, and H. Knoeff. 2011. "Fine-Tuning of the Backward Erosion Piping Model through Small-Scale, Medium-Scale and IJkdijk Experiments." European Journal of Environmental and Civil Engineering 15 (8): 1139–54. doi:10.1080/19648189.2011.9714845.

Sellmeijer, J. B. 1988. "On the Mechanism of Piping under Impervious Structures." Dissertation, Netherlands: TU Delft.

Van Beek, V., A. Bezuijen, J. B. Sellmeijer, and F.B.J. Barends. 2014. "Initiation of Backward Erosion Piping in Uniform Sands." Geotechnique, December. doi:http://dx.doi.org/10.1680/geot.13.P.210.

Van Beek, V., H.T.J. de Bruijin, J. G. Knoeff, A. Bezuijen, and U. Forster. 2010. “Levee Failure Due to Piping: A Full-Scale Experiment.” In Scour and Erosion GSP 210. San Francisco, CA. http://scitation.aip.org/getabs/servlet/GetabsServlet?prog=normal&id=ASCECP0003920411470 00027000001&idtype=cvips&gifs=yes.

Van Beek, V., H. de Bruijn, and H. Knoeff. 2009. SBW Piping: Piping Revalidation, Full-Scale Tests, Factual Report Experiment 2 (SBW Piping: Hervalidatie Piping HP5.4b Full-Scale Proeven (factual Report Proef 2)). 1200690-005-GEO-0005. Deltares.

Van der Kolk, B. 2013. Research into the Action of Geotextiles as Piping Inhibitory Action (Onderzoek Naar de Werking van Geotextielen Als Pipingremmende Maatregel). 1206806-006-GEO-0001. Deltares.

Zwanenburg, C., E. J. Den Hann, G. A. M. Kruse, and A. Koelewijn. 2012. “Failure of a Trial Embankment on Peat in Booneschans, the Netherlands.” Geotechnique 62 (6): 479–90.